

# SEISMIC EVENT LOCALISATION BASED ON CROSS-CORRELATION STACKING

*M. Behzadi, D. Gajewski and C. Vanelle*

**email:** *mehrnoosh.behzadi@studium.uni-hamburg.de*

**keywords:** *localisation, passive seismic, microtremor, cross-correlation, acquisition footprint, seismic imaging*

## ABSTRACT

*Passive seismic methods are of high interest to the petroleum industry. Since the acquisition geometry often follows a sparse irregular pattern, the results are often contaminated by acquisition artifacts. In this study, we suggest a passive seismic imaging method based on zero lag cross-correlation and stacking to localise the elastic emissions. The method uses all recorded channels simultaneously, which allows to detect even very small events. The maximum value of the image obtained by this method provides the source location. To achieve a more highly-resolved image, an alternative algorithm based on Voronoi polygons is proposed to countermand the effect of the acquisition footprint. Furthermore, effects due to geometrical spreading are compensated during the localisation procedure. Thus weighting the data results in a better focussed image function with lower noise. However, it can also lead to artificial focusing in the image. Synthetic and field data examples demonstrate the new method's robustness and its potential for real time monitoring of the subsurface.*

## INTRODUCTION

For the past four decades, the earth's seismic ambient noise has been used extensively for sedimentary basin studies and, particularly, seismic hazard and microzonation studies. Nevertheless, only in the past ten years have passive seismic techniques, applicable to microseismic events and seismic ambient noise, gained growing interest for hydrocarbon exploration, scientifically as well as economically (Emidio and Nunes, 2010; Graf et al., 2007; Saenger et al., 2007). They do not require artificial sources or large number of personnel, therefore the costs are low. Furthermore, they can be used in sensitive environments where conventional seismic methods face problems (Emidio and Nunes, 2010). Although passive seismic sources are currently monitored and studied (Graf et al., 2007; Steiner et al., 2008; Ryberg et al., 2010; Emidio and Nunes, 2010; Zhebel et al., 2011; Eisner et al., 2011), a high resolution imaging process that can detect very weak events has yet to be properly explored.

Recently, passive seismic methods have even been suggested as a tool to detect a direct hydrocarbon indicator (Steiner, 2009; Lambert et al., 2009; Graf et al., 2007; Saenger et al., 2007). The latter use empirical observations of an increase in the ambient seismic noise's spectral energy at a frequency range around 1 to 6 Hz in the presence of hydrocarbons. Such frequency anomalies have been observed above several hydrocarbon reservoirs but not outside the reservoir area. Although the origin of the spectral anomalies is yet unexplained, a possible source could be the resonant oscillation of oil and gas within the reservoir (Steiner, 2009). This phenomenon represents a low-frequency event that is also referred to as a microtremor. Microtremors continuously emit seismic energy from the source area over a duration of hours to weeks. In contrast, classical seismic events like earthquakes last for seconds. Microtremor events are also observed in volcanic areas and in several subduction zones. In particular, non-volcanic tremors (NVT) are characterised by low amplitudes, lack of energy at high frequencies, coherent envelopes, emergent onsets, and

the absence of clear impulsive phases. Their durations last from minutes to days (Obara, 2002; Obara and Hirose, 2006; Ghosh et al., 2009).

The ability to localise the origin of microtremor events would thus be helpful in seismology, volcanology, and hydrocarbon studies. However, since microtremor events are continuous in time, they can not be picked. The localisation of microtremors therefore requires other techniques than those applicable for classical seismic events (Graf et al., 2007; Ghosh et al., 2009). Imaging or back projection methods, as used for active seismic data, have not yet fully exploited their potential as microtremor localisation techniques but can be considered as a starting point for such a technique.

Gajewski and Tessmer (2005) introduced a localisation method based on reverse time modelling, which does not require any picking of events and uses all recordings simultaneously. The advantage of this method is that the energy is focused during the back projection process, which allows to image even very weak events that can not be identified in an individual seismogram of the recording network. Later, Gajewski et al. (2007) proposed a new technique based on a diffraction stacking approach to back project passive seismic observations, where the subsurface is discretised and each subsurface point is considered as a potential location of a seismic event. Zhebel (2013) extended the diffraction stacking method as a suitable tool to locate the origin of seismic events even when the signal-to-noise ratio (SNR) is rather poor. She studied the impact of the acquisition geometry and propagation effects as well as several imaging conditions. However, these works have not yet been applied to continuous signals.

Steiner et al. (2008) applied time reverse modelling (TRM) to image microtremor events to the subsurface. Their idea of locating the spatial origin of signals with TRM has been adapted from existing studies by other authors in physics, medicine and seismology. Of the various methods in TRM to collapse the time axis, the so-called imaging condition, Steiner et al. (2008) used the absolute particle displacement or velocity per grid point throughout the entire time of the reverse modelling. In this imaging condition, the highest values correspond to either the highest amplitude of one wave front or to the positive interference of recorded signals, which were reversely propagated to the corresponding subsurface locations.

This study deals with the development and the application of a seismic imaging method based on cross-correlation stacking as a numerical tool to locate microtremor episodes. An algorithm based on Voronoi cells is suggested to countermand the effect of the acquisition footprint and the geometrical spreading is compensated during the procedure. After introducing the theory in the following section, we evaluate the method with impulsive sources in synthetic data and NVT's from the Cascadia subduction zone. In both cases, the results confirm the good performance of the technique.

## METHOD

In this section, we outline the basic principle of imaging based on cross-correlation stacking. We then discuss the potential use of different components if 3C data are available. Finally, we address the removal of the acquisition footprint and compensation of geometrical spreading.

### Cross-correlation stacking based imaging

Cross-correlation is a measure of the similarity of two waveforms as a function of a time-lag between them. This property is exploited in the localisation method that we describe in the following.

We consider a discretised subsurface, where each node of the grid represents a potential source location. The nodes are called image points in the following. The traveltimes from each image point to each receiver locations of the recording network are calculated with an a priori determined velocity model. For each image point the receiver with the shortest traveltimes is selected. This receiver represents the apex location of the corresponding traveltimes curve and its traveltimes is denoted zero time  $\tau_0$ . Based on the zero time, the moveout at the other receiver locations is determined and applied as a static shift to the input seismograms. For a consistent velocity model, the events should align after applying this static moveout shift.

In the next step, a zero lag cross-correlation is carried out to collapse the time axis of the considered time window. This step represents the imaging condition. In this process any trace can be considered as the master trace for the correlation. Finally, all cross-correlation results are stacked over all offsets, thus leading to the amplitude assigned to the image point under consideration. Repeating the procedure for all image points provides the image function or section.

### Localisation with three-component measurements

If three components were registered, several options exist to apply the procedure introduced in the previous section. In the simplest case, the localisation is carried out component-wise, e.g., only the vertical component (V) is considered at all. Another option is to stack the horizontal and vertical images (H+V). Finally, the image function obtained from the horizontal components can be normalised by the vertical image function (H/V). This imaging condition is referred to as scaled horizontal by vertical images in the seismological literature (see, e.g., Nakamura, 1989).

### Acquisition footprint

The acquisition pattern of a survey can have a significant effect on the imaging result (see, e.g., Canning and Gardner, 1998): when the spatial distribution of the input traces is irregular, the localisation results is often contaminated by artifacts. This so-called acquisition footprint can lead to inaccurate interpretation of images and is a well-known problem in passive seismics where sparse and irregular networks are more common than in active experiments. A possible solution is the application of weight functions to account for the irregular spacing (Canning and Gardner, 1998; Zhebel, 2013).

For the weight we use in this work, we determine the effective area covered by each receiver. The size of this region is calculated from the associated Voronoi cell (Voronoi, 1908), the area bounded by perpendicular bisectors to all adjacent receivers (see Figure 2). The resulting area is assigned as the weight for the receiver under consideration.

### Propagation effects

The measured amplitudes of seismic events are not only affected by the acquisition footprint described above and the source strength but also by propagation effects like the reflection and transmission at boundaries and wavefront divergence. The latter is also known as geometrical spreading and can be taken into account during the localisation procedure. Of the many approaches to compute geometrical spreading factors (for an overview, see, e.g., Vanelle and Gajewski, 2003), we chose a weight function that is closely related to the expression by Newman (1973).

In the next section, we present results of our method from application to 3D synthetic data with impulsive sources and field data in the presence of NVT's. We investigate the performance of the acquisition footprint removal and geometrical spreading compensation as well as the behaviour of the imaging condition depending on the considered components.

## EXAMPLES

### Synthetic data with impulsive sources

Steiner (2009) constructed a complex heterogeneous velocity model suited for synthetic event localisation studies. We have extended his model, which simulates a reservoir near Voitsdorf, Austria, to 2.5D. The model consists of ten sedimentary layers with P-wave velocities between 1200 and 3000 m/s above a crystalline basement with a P-wave velocity of 6000 m/s (see Figure 1). The S-wave velocities are derived from the P-wave velocities with a constant  $V_P/V_S$ -ratio of 1.633. Figure 2 illustrates the recording array consisting of 31 irregularly placed seismometers and the corresponding Voronoi polygons. The horizontal and vertical particle velocities are recorded until 4 s.

Synthetic seismograms were generated with NORSAR Ray Modelling for two experiments that both use a horizontal single force source. In the first experiment, the source was positioned at (6600 m, 1500 m, 1500 m). The epicentre was thus inside the aperture, which leads to a good coverage. The second experiment placed the source at (1500 m, 2200 m, 1200 m) at the border of the aperture with minimal coverage by the recording array. In both cases, a Ricker wavelet with a 10 Hz main frequency was used as a source time function. Noise with a signal-to-noise ratio (SNR) of about 5 was added to the data.

The localisation procedure was applied using P and S-wave first arrival traveltimes, also provided by NORSAR Ray Modelling, for both experiments. Figure 3 demonstrates the localisation images of the event

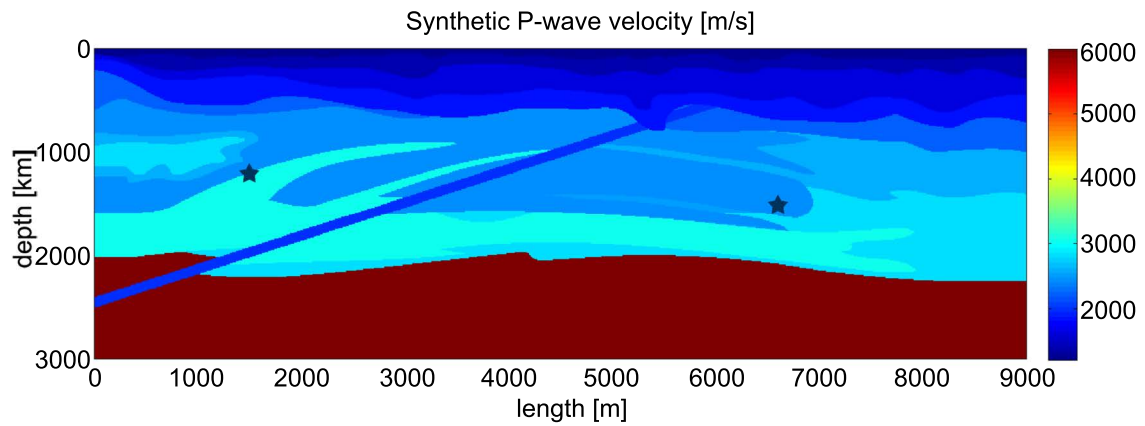


**Figure 1:** Synthetic example: the 2.5D velocity model consists of ten sedimentary layers above a basement unit (Steiner, 2009). Two black stars indicate the source positions in the  $x - z$ -plane.

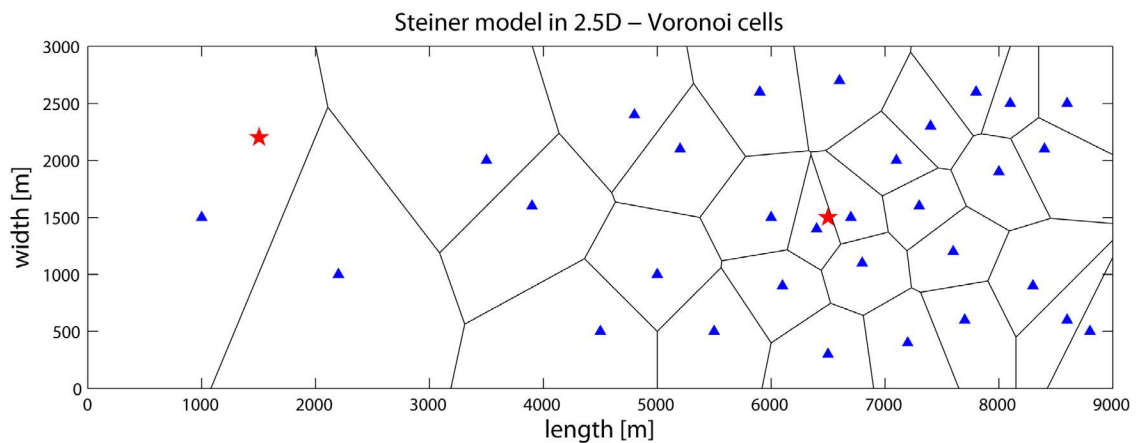


**Figure 2:** Synthetic example: 2-D surface array for the Steiner model. Blue triangles denote the 31 seismometers. The polygons mark the associated Voronoi cells. The two red stars indicate the epicentres of the microseismic events.

set within the aperture, without and with removal of the acquisition footprint and compensation for geometrical spreading. We recognise a well focussed image with a maximum at the real source position with no significant improvement by considering acquisition footprint and geometrical spreading. The results for the event at the border of the array are shown in Figure 4. Again, we find well focussed image functions with the maximum at the real source position. However, the image without the correction displays a higher noise level as well as artificial focusing effects. In this case, the correction has improved the localisation/

In Figure 5, we investigate the influence of the acquisition footprint and geometrical spreading in more detail. It displays the amplitude profiles of the image function in  $x$ - and  $y$ -direction, taken at the real depth of the respective source. We observe for both events that although the geometrical spreading correction leads to higher amplitudes, the removal of the acquisition footprint has a larger impact.

Now that we have shown that the method performs well for the localisation of an impulsive source, we will investigate it for field data with continuous signals in the next section.

### Application to field data with continuous signals

In our field data example, we attempt to localise deep non-volcanic tremors (NVT) in the Cascadia subduction zone. The P-wave velocity model derived by Preston (2003) is shown in Figure 6. For the computation of S-wave velocities we have assumed constant  $V_P/V_S$ -ratio of  $\sqrt{3}$ .

The data were provided by USGS/NEIC, who collected continuous microtremor recordings from the IRIS networks. The network consist of 53 stations with three-component sensors that record data with a sampling interval of 25 ms in continuous mode. Figure 7 shows the survey design.

After bandpass filtering the data, we have carried out the localisation for 30 minute time buffers using a sliding time window of 5 minutes length. We have localised several events that occurred between November 2012 and January 2013.

To further constrain the event detection, a visual estimation of frequency anomalies was applied by analysing the spectrograms of each trace. For this investigation, we selected time windows with a well focussed spectrum. Figure 8 demonstrates three recordings at different stations, and their corresponding spectrograms. A distinct maximum in a spectrogram indicates the existence of NVT's during the half-hour respective time window, although the event is too weak to be visible in the individual seismogram.

In order to investigate the influence of the considered components, we have chosen an event that was also detected by the USGS/NEIC. According to their earthquake catalogue, it occurred at Lat/Lon  $45.35^\circ$ – $123.2^\circ$  and a depth of 23.3 km on January 19th, 2013, at 02:35:28 with a Magnitude of 2.3 ML.

Figure 9 shows the localisation results after acquisition footprint removal and geometrical spreading compensation. White stars indicate the source position determined by USGS/NEIC. We observe in Figure 9(a) that use of the vertical component leads to strong artifacts. Localisation by stacking of horizontal and vertical image functions (Figure 9(b)) results in even more artifacts with the highest amplitude at an entirely wrong location. Finally, normalising the horizontal image function by the vertical one provides an image that is well focused and displays considerably less artifacts, as can be observed in Figure 9(c).

Finally, we present a map of the tremor epicentres located by our method during the November 2012 to January 2013 period in Figure 10. Only strong detections are shown. The source time is colour-coded to illustrate temporal evolution. Even though tremors are generally hard to detect due to their lack of clear impulsive arrivals, Figure 10 shows that the main tremor activity is observed near the plate interface, suggesting that the tremors in this region may be a result of shear slip on the subduction fault. In any event, our results demonstrate that our method provides a reliable localisation also for continuous signals.

## CONCLUSIONS

In this study, we presented a passive seismic imaging method based on cross-correlation for localisation of elastic emissions. The method does not require event picking and uses all channels of a three-component experiment simultaneously. Furthermore, it allows to correct for propagation effects in terms of geometrical spreading and removal of the acquisition footprint, which can lead to artifacts and artificial focusing in the resulting image function.

Our examples on synthetic and field data demonstrate that the method performs well for impulsive as well as continuous signals and the removal of the acquisition footprint and geometrical spreading leads to

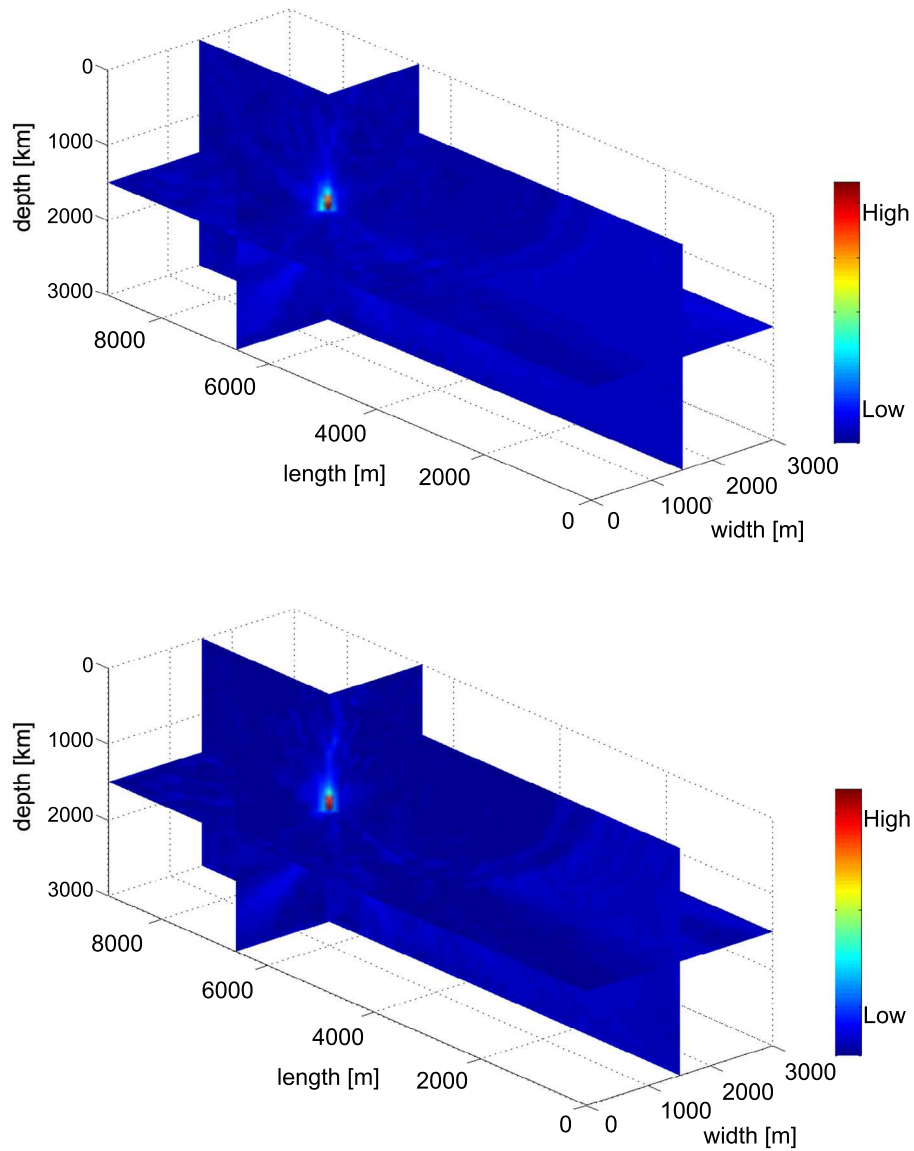


**Figure 3:** Synthetic example: image functions for an impulsive point source event within the aperture. Top: without correction for the acquisition footprint and compensation for geometrical spreading; bottom: after the corrections were applied. The maximum value of the image corresponds to the source location.

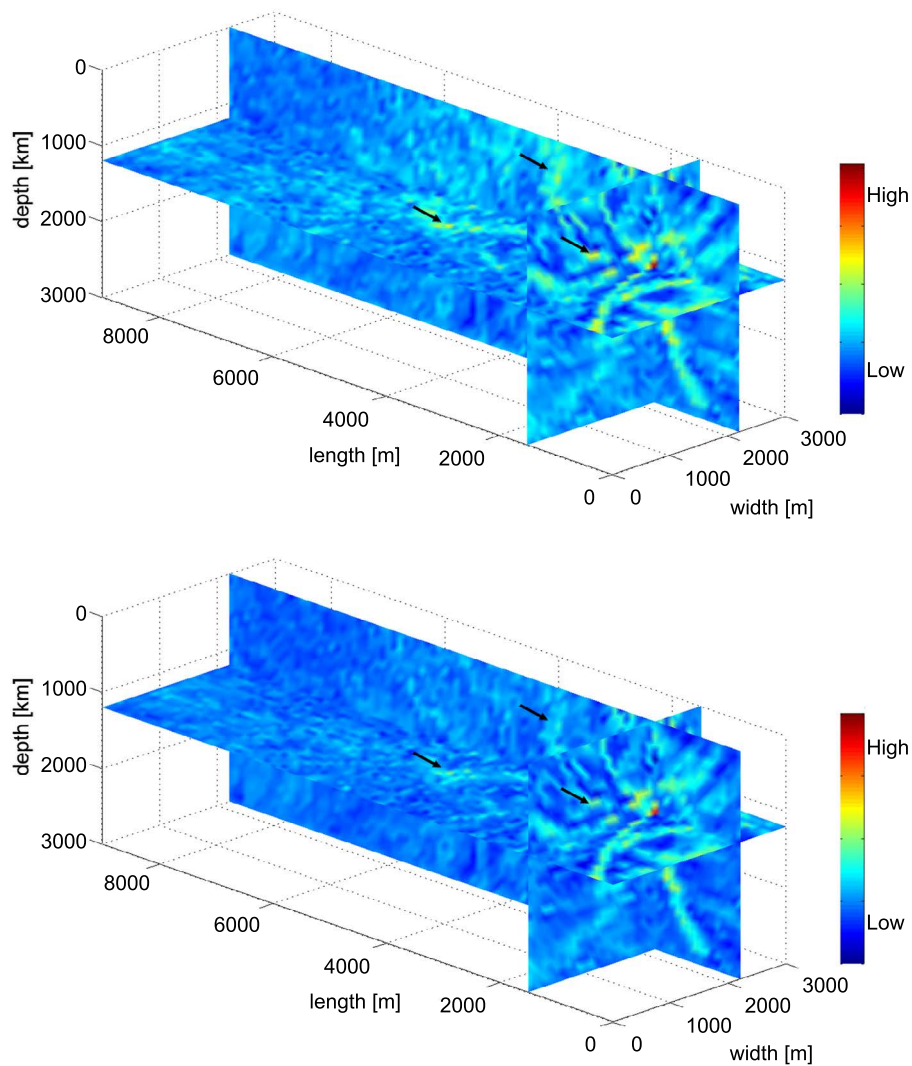


**Figure 4:** Synthetic example: image functions for an impulsive point source event at the border of the aperture. Top: without correction for the acquisition footprint and compensation for geometrical spreading; bottom: after the corrections were applied. The maximum value of the image corresponds to the source location.

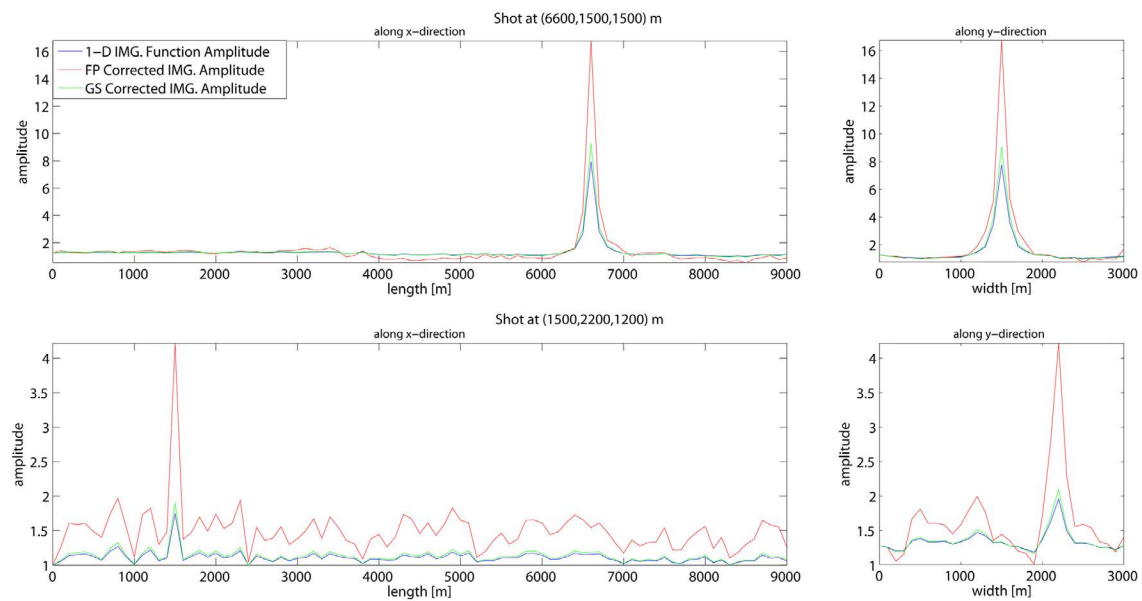


**Figure 5:** Synthetic example: influence of acquisition footprint removal (FP) and geometrical spreading correction (GS) on the amplitudes of the image functions. Sections are taken through the respective correct source position. The amplitudes without any correction are shown for comparison. The top figure corresponds to the impulsive point source located within the aperture of the experiment; the bottom figure depicts the behaviour for an event at the border of the aperture.

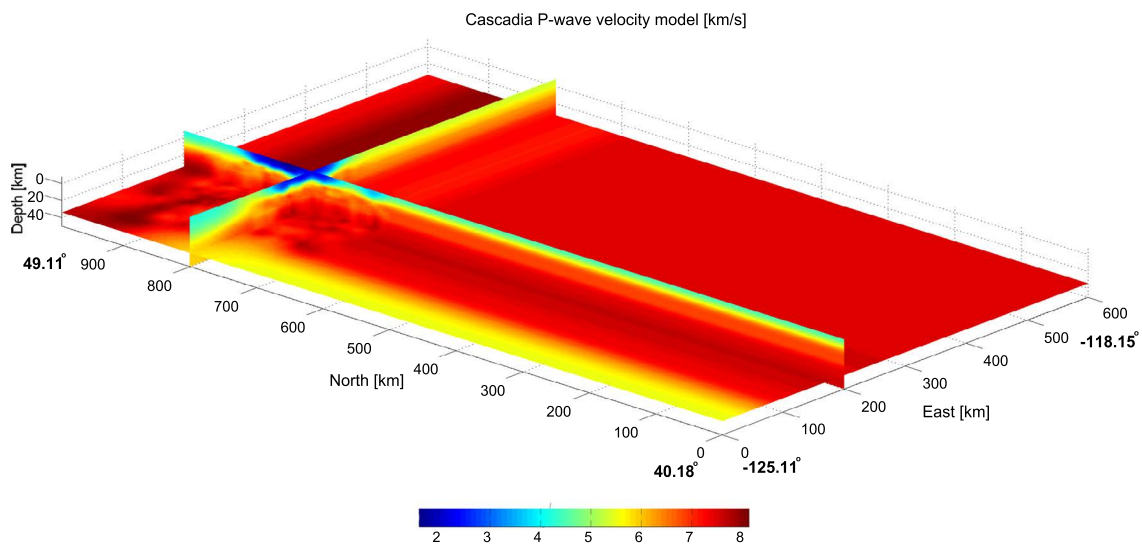


**Figure 6:** Field data example: the Cascadia velocity model was derived from 3D seismic tomography by Preston (2003). The legend shows the P-wave velocity in km/s.

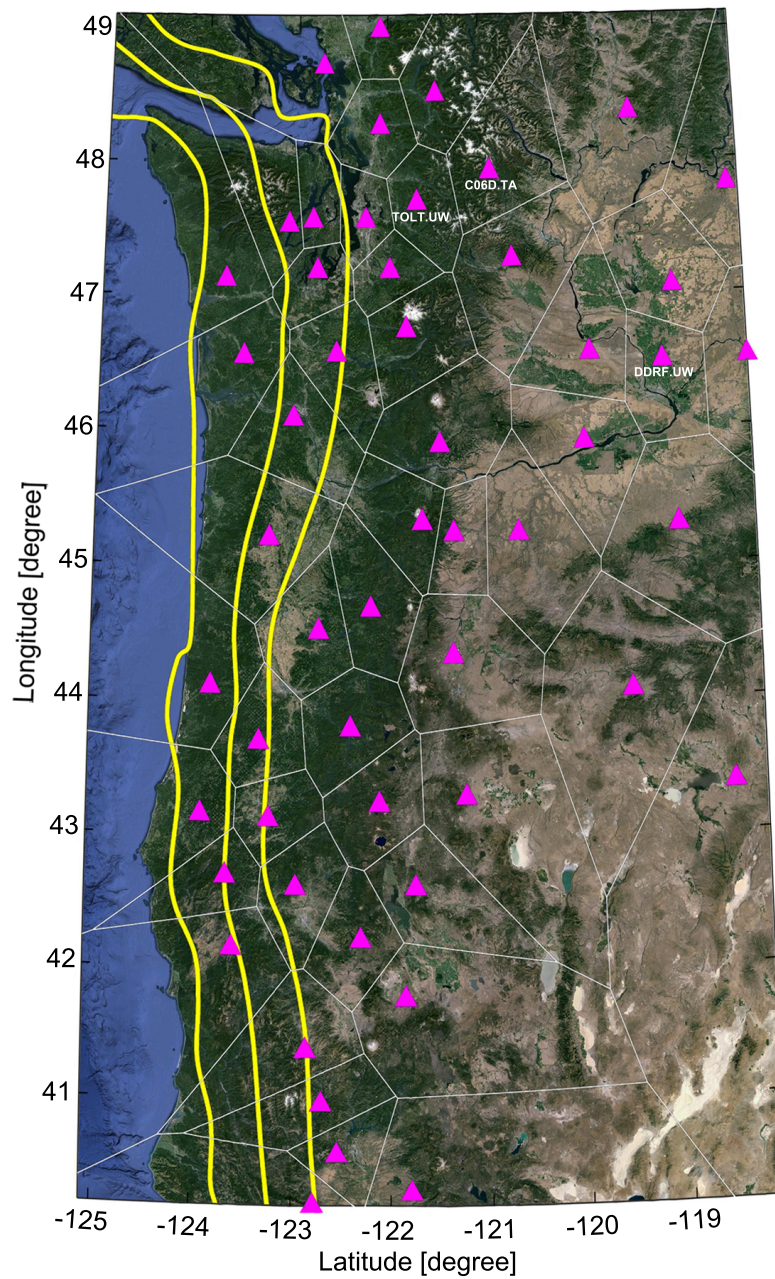


**Figure 7:** Field data example: the surface array consisting of 53 seismometers (magenta triangles) is shown together with the associated Voronoi polygons. The yellow lines indicate the isolines of 20, 30 and 40 km depth of the slab above a low velocity zone (LVZ) along the Cascadia margin (McCrorry et al., 2006).

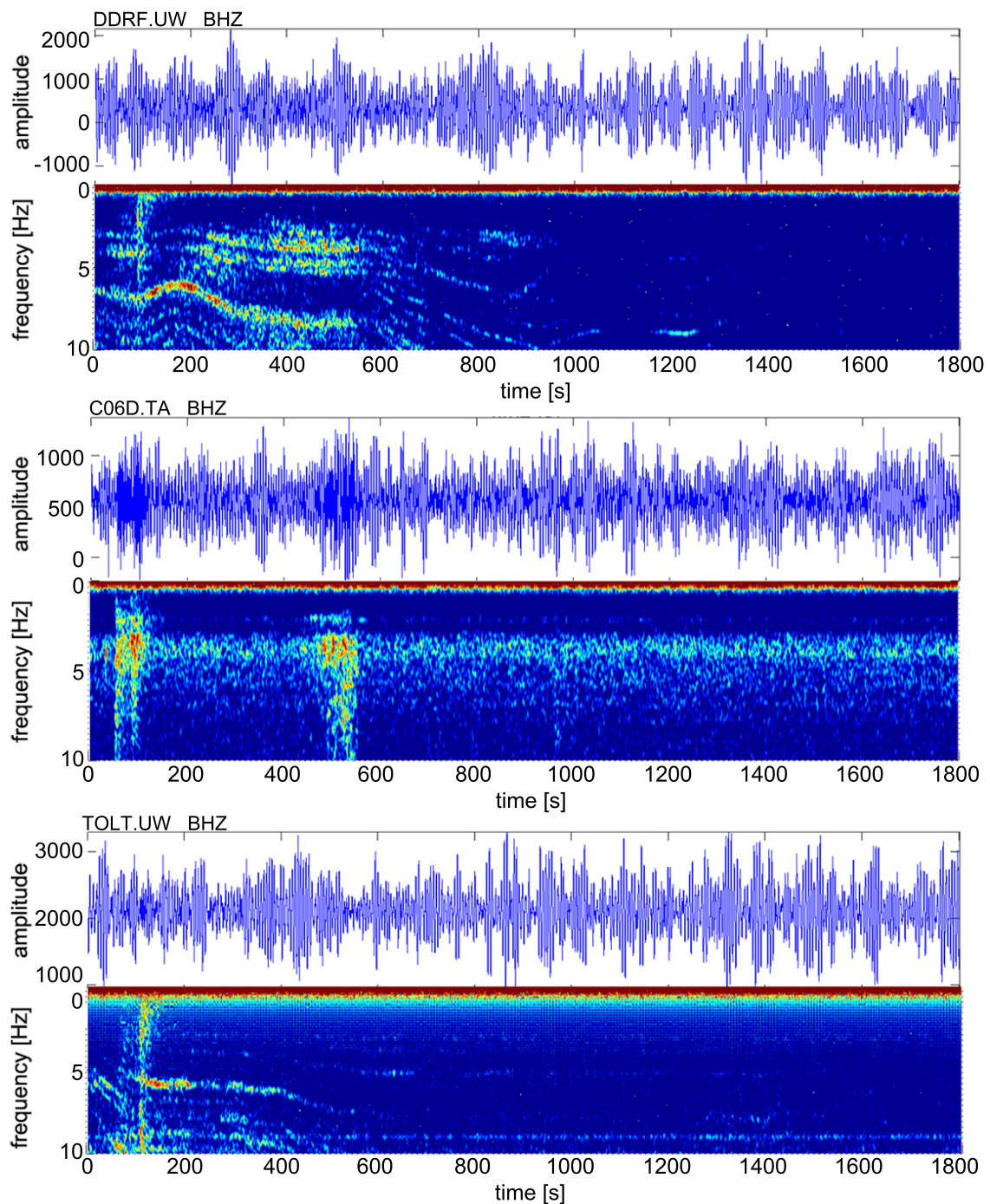


**Figure 8:** Field data example: visual estimation of NVT detection on 19th November 2012 at 14:15:00. Vertical component recordings at three different stations and their corresponding spectrograms are shown. The amplitudes (given in db) increase from cool to hot colours. Maxima in the spectrograms indicate the existence of NVT's during the displayed half hour time window.

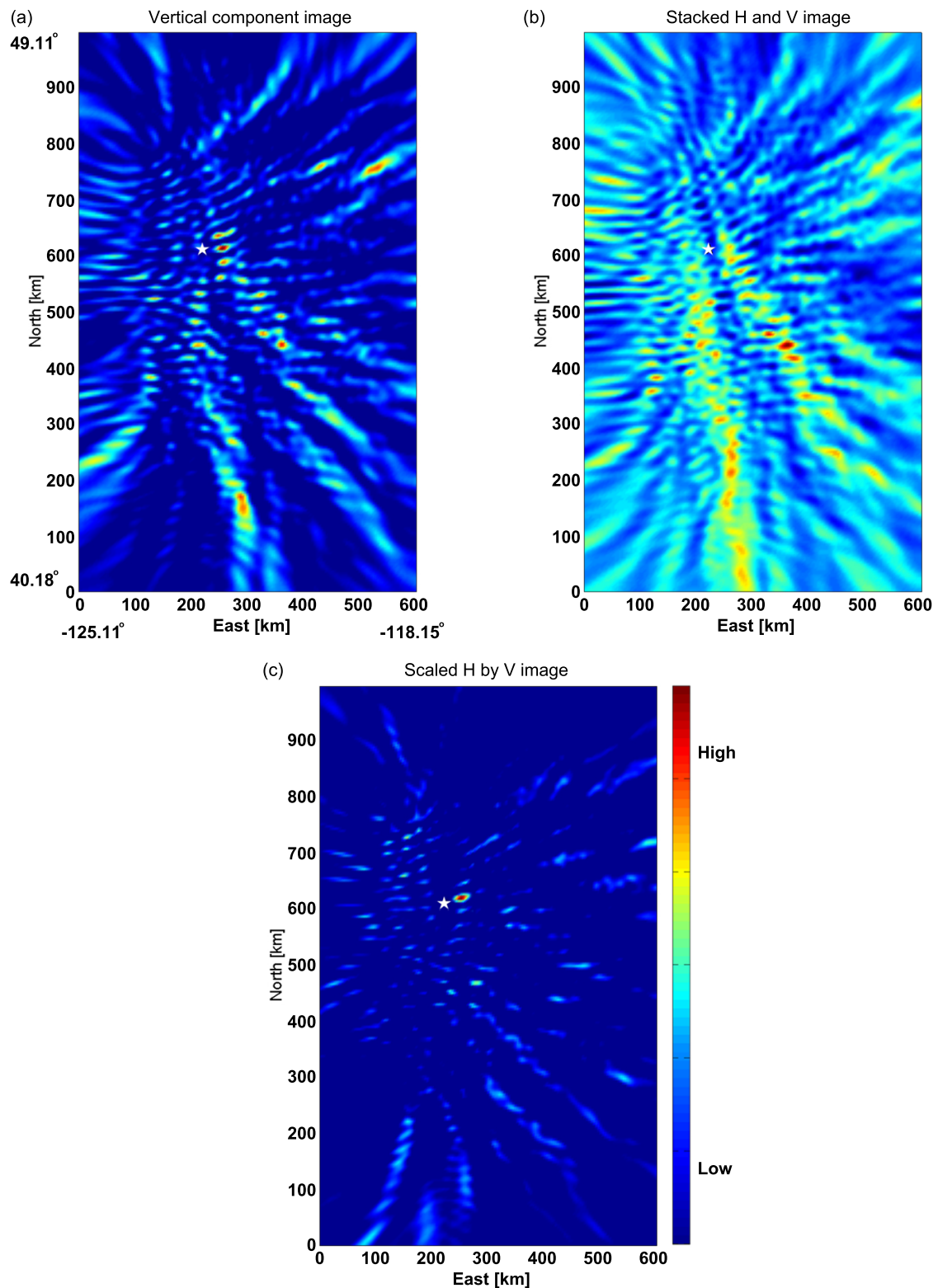


**Figure 9:** Field data example: normalised horizontal sections taken at the localised event depth ( $z=24$  km) for an NVT event in Cascadia on 19th January 2013: (a) vertical, (b) stacked horizontal and vertical, and (c) scaled horizontal to vertical image function. Acquisition footprint reduction and geometrical spreading compensation were applied prior to the localisation procedure. The white stars in the images indicate the source location suggested by USGS/NEIC.

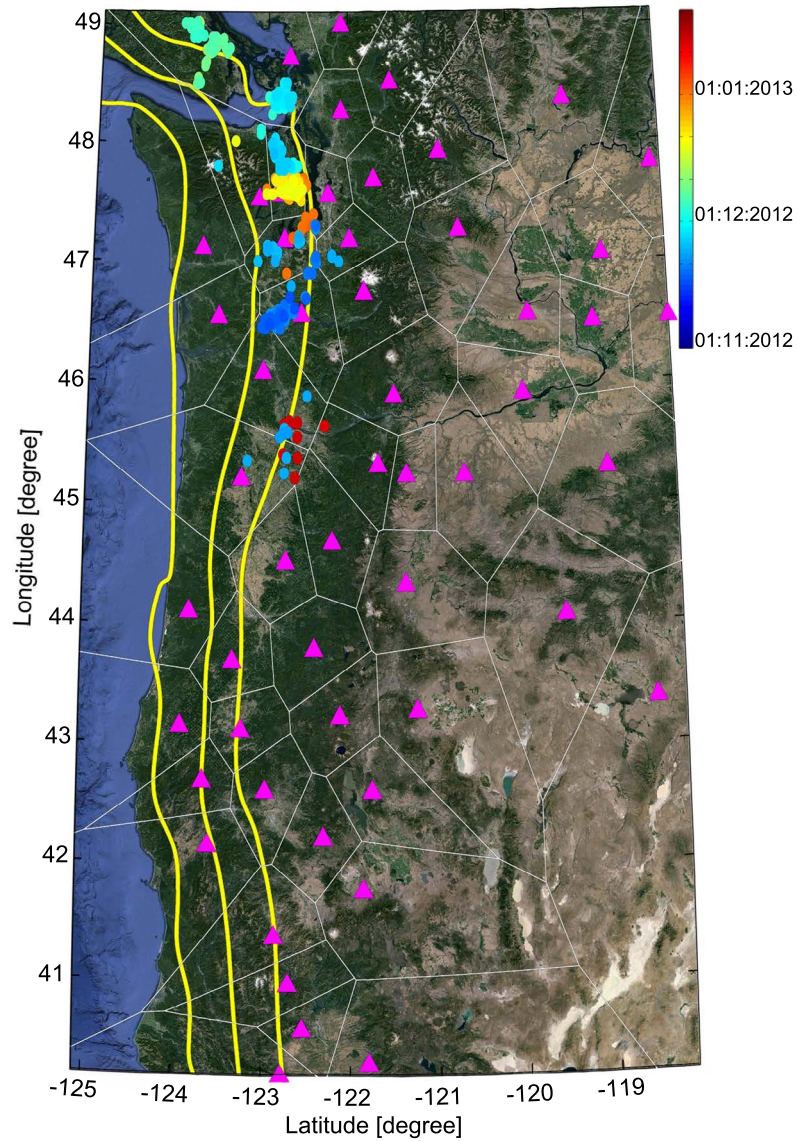


**Figure 10:** Field data example: Satellite image of the Cascadia subduction zone and overlaid tremor epicentres during the period from November 2012 to January 2013. Only strong detections are shown with their source time coded by colour.

a considerable improvement of the localisation in terms of a better signal-to-noise ratio and well-focused source position. Further investigation of the three-component field data suggests that an imaging condition that considers horizontal image functions normalised by the vertical one provides the best results. This conclusion is, however, tentative, as it depends strongly on the source type and S-wave contributions in the data.

#### ACKNOWLEDGEMENTS

We thank the applied seismics group in Hamburg for continuous discussions. Marie Voß kindly proof-read the manuscript. We are grateful to Brian Steiner, Proseis AG, for providing the model and synthetic microtremor data, as well as to Leiph Alexander Preston, Sandia National Laboratories, who provided the tomographic velocity model for the Cascadia region. NORSAR 3D was applied to generate traveltimes tables. This research was supported by University of Hamburg and the sponsors of the WIT consortium.

#### REFERENCES

- Canning, A. and Gardner, G. H. F. (1998). Reducing 3-D acquisition footprint for 3-D DMO and 3-D prestack migration. *Geophysics*, 63:1177–1183.
- Eisner, L., De La Pena, A., Wessels, S., Barker, W. B., and Heigl, W. M. (2011). Why surface monitoring of microseismic events works. In *Expanded Abstracts*, page PAS10.
- Emidio, A. and Nunes, L. (2010). Pitfalls of tremor-like signals for hydrocarbon exploration in producing oil fields in Potiguar Basin, northeast Brazil. *The Leading Edge*, 7:826–830.
- Gajewski, D., Anikiev, D., Kashtan, B. M., Tessmer, E., and Vanelle, C. (2007). Source location by diffraction stacking. In *Expanded Abstracts*, page P215.
- Gajewski, D. and Tessmer, E. (2005). Reverse modeling for seismic event characterization. *Geophysical Journal International*, 163:276–284.
- Ghosh, A., Vidale, J. E., Sweet, J. R., Creager, K. C., and Wech, A. G. (2009). Tremor patches in Cascadia revealed by seismic array analysis. *Geophysical Research Letters*, 36(L17316).
- Graf, R., Schmalholz, S. M., Podladchikov, Y., and Saenger, E. H. (2007). Passive low frequency spectral analysis: Exploring a new field in geophysics. *World Oil*, 228:47–52.
- Lambert, M. A., Schmalholz, S. M., Saenger, E. H., and Steiner, B. (2009). Low-frequency microtremor anomalies at an oil and gas field in Voitsdorf, Austria. *Geophysical Prospecting*, 57:393–411.
- McCrory, P. A., Blair, J. L., Oppenheimer, D. H., and Walter, S. R. (2006). Depth to the Juan de Fuca slab beneath the Cascadia subduction margin: A 3-D model for sorting earthquakes. Data series 91 version 1.2, USGS Data Service.
- Nakamura, Y. (1989). A method for dynamic characteristics estimation of subsurface using microtremor on the ground surface. *Quarterly Report of RTRI*, 30(1):25–33.
- Newman, P. (1973). Divergence effect in a layered earth. *Geophysics*, 38:481–488.
- Obara, K. (2002). Nonvolcanic deep tremor associated with subduction in southwest Japan. *Science*, 296:1679–1681.
- Obara, K. and Hirose, H. (2006). Non-volcanic deep low-frequency tremors accompanying slow slips in the southwest Japan subduction zone. *Tectonophysics*, 417:33–51.
- Preston, L. A. (2003). *Simultaneous inversion of 3D velocity structure, hypocenter locations, and reflector geometry in Cascadia*. PhD thesis, University of Washington.

- Ryberg, T., Haberland, C., Fuis, G. S., Ellsworth, W. L., and Shelly, D. R. (2010). Locating non-volcanic tremor along the San Andreas Fault using a multiple array source imaging technique. *Geophysical Journal International*, 183(3):1485–1500.
- Saenger, E. H., Torres, A., Rentsch, S., Lambert, M., Schmalholz, S. M., and Mendez-Hernandez, E. (2007). A hydrocarbon microtremor survey over a gas field: Identification of seismic attributes. In *Expanded Abstracts*, pages 1277–1281. SEG Annual Meeting.
- Steiner, B. (2009). *Time reverse modeling of low-frequency microtremors*. PhD thesis, ETH Zurich.
- Steiner, B., Saenger, E., and Schmalholz, S. (2008). Time reverse modeling of low-frequency microtremors: Application to hydrocarbon reservoir localization. *Geophysical Research Letters*, 35(L03307).
- Vanelle, C. and Gajewski, D. (2003). Determination of geometrical spreading from traveltimes. *Journal of Applied Geophysics*, 54:391–400.
- Voronoi, G. F. (1908). Nouvelles applications des paramètres continus à la théorie de formes quadratiques. *Journal für die reine und angewandte Mathematik*, 134:198–287.
- Zhebel, O. (2013). *Imaging of seismic events. The role of imaging conditions, acquisition geometry and source mechanisms*. PhD thesis, Universität Hamburg.
- Zhebel, O., Gajewski, D., and Vanelle, C. (2011). Localization of seismic events in 3D media by diffraction stacking. In *Expanded Abstracts*, page C005.